

Leveraging phenotypic plasticity in seed oil content for climate-adapted breeding and production

Tingting Guo¹, Lingju Zeng¹, Xu Han¹, Xiangjian Gou¹, He Pei¹, Yang Shao¹, Yilan Cao¹, Zhenwei Zhang¹, Xianran Li², Jianming Yu³, Jianbing Yan¹, and Liang Guo¹

¹National Key Laboratory of Crop Genetic Improvement

²USDA Agricultural Research Service Wheat Health Genetics and Quality Research Unit

³Iowa State University of Science and Technology Department of Agronomy

April 26, 2024

Abstract

Phenotypic plasticity is the ability of organisms to respond to environmental changes. Understanding and leveraging crop phenotypic plasticity is crucial for mitigating the threats caused by climate change. Here, we assessed phenotypic plasticity in multi-environment trials over 4 years, covering a wide geographical area, using 505 inbred lines from a *Brassica napus* genetic diversity panel. The observed phenotypic variation for seed oil content (SOC) was influenced by three environmental indices (precipitation, diurnal temperature range, and ultraviolet B) during the flowering or pod-filling stage alongside five plasticity genes. Leveraging this information with climate records, we developed a predictive model to estimate SOC for various planting dates in seven major production regions, and validated the accuracy of our predictions in new environments. With the quantified plasticity conferred by genetic variation in the five plasticity genes, we identified an optimal haplotype for each production region for adaptability to future climate projections. This study offers valuable insights and selection of materials to mitigate the adverse effects of climate change on agriculture.

Leveraging phenotypic plasticity in seed oil content for climate-adapted breeding and production

Lingju Zeng^{1,2*}, Xu Han^{1,2*}, Xiangjian Gou^{1,2}, He Pei^{1,2}, Yang Shao^{1,2}, Yilan Cao^{1,2}, Zhenwei Zhang^{1,2}, Xianran Li⁵, Jianming Yu⁴, Jianbing Yan^{1,2,3}, Liang Guo^{1,2,3*}, Tingting Guo^{1,2*}

Affiliations :

¹National Key Laboratory of Crop Genetic Improvement, Huazhong Agricultural University, Wuhan, 430070, China

²Hubei Hongshan Laboratory, Wuhan, 430070, China

³Yazhouwan National Laboratory, Sanya, 572025, China

⁴Department of Agronomy, Iowa State University, Ames, IA 50011, USA

⁵USDA, Agricultural Research Service, Wheat Health, Genetics, and Quality Research Unit, Pullman, WA 99164, USA

Correspondence :

Tingting Guo, email: tguo@mail.hzau.edu.cn

Liang Guo, email: guoliang@mail.hzau.edu.cn

Competing interest:

The authors declare no conflict of interest.

Data availability:

All data are included in the manuscript and its supplementary file. Data for phenotype are provided in Supplementary Tables S3–S4. Data for weather information are provided in Supplementary Tables S10–S14.

Additional information:

Supplementary data:

The following supplementary data are available for this article:

Supplementary Figure S1 – S13

Supplementary Table S1 – S17

Funding information:

This study was supported by the National Natural Science Foundation of China (32225037, 32301839).

Highlights (1-2 sentences):

This study analyzes phenotypic plasticity to identify environmental indices, genes, and their modes of action, and uses this information to predict ideal planting dates for different environmental conditions and determine the optimal haplotypes for future climates.

Abstract:

Phenotypic plasticity is the ability of organisms to respond to environmental changes. Understanding and leveraging crop phenotypic plasticity is crucial for mitigating the threats caused by climate change. Here, we assessed phenotypic plasticity in multi-environment trials over 4 years, covering a wide geographical area, using 505 inbred lines from a *Brassica napus* genetic diversity panel. The observed phenotypic variation for seed oil content (SOC) was influenced by three environmental indices (precipitation, diurnal temperature range, and ultraviolet B) during the flowering or pod-filling stage alongside five plasticity genes. Leveraging this information with climate records, we developed a predictive model to estimate SOC for various planting dates in seven major production regions, and validated the accuracy of our predictions in new environments. With the quantified plasticity conferred by genetic variation in the five plasticity genes, we identified an optimal haplotype for each production region for adaptability to future climate projections. This study offers valuable insights and selection of materials to mitigate the adverse effects of climate change on agriculture.

Keywords: phenotypic plasticity; climate change; plant breeding; planting date; germplasm; haplotype

Introduction

Climate change is increasingly threatening global food security (Lesk et al., 2022). Many regions have already witnessed significant yield losses caused by shifting temperatures and changing weather patterns. These losses are projected to worsen in the future (Tigchelaar et al., 2018, Fu et al., 2023). To ensure the stability of crop production systems, climate-aware strategies should be prioritized in breeding and agronomy (Hickey et al., 2019, Zhao et al., 2022). As a first step, a solid understanding of how climate change affects crop performance and of the genetic mechanisms underlying crop responses is thus essential before developing efficient and effective strategies in breeding and agronomic practices. When combined with innovative technologies, these strategies are expected to play a central role in addressing the challenge of crop adaptability to future climates.

Phenotypic plasticity, or the ability to alter performance in response to environmental conditions, is a fundamental characteristic of plants, including crops (Pigliucci et al., 2006), that enables them to thrive in diverse environments (Bonamour et al., 2019, Xue and Leibler, 2018). To harness this mechanism to

enhance crop performance in changing environments, numerous studies have investigated the molecular basis of phenotypic plasticity across various traits, species, and environments (Liu et al., 2020, Kusmec et al., 2017). Genes that underlie phenotypic plasticity have been identified, and their effects have been shown to be dynamic across different environments (Des Marais et al., 2013, Li et al., 2018). Moreover, environmental factors that interact with genes to determine the overt phenotypes have been examined using algorithms such as Critical Environmental Regressor through Informed Search (CERIS) (Li et al., 2021, Li et al., 2022). Progress has also been made in determining the developmental patterns behind phenotypic plasticity (Mu et al., 2022). While these findings have expanded our understanding of phenotypic plasticity, it is crucial to use this knowledge to streamline strategies for helping crops adjust to current and future climate change.

Brassica napus (*B. napus*) is a valuable crop in which phenotypic plasticity can be explored in the context of climate change. Compared to other seed crops, *B. napus* is less tolerant to water deficit and high temperature, highlighting the significant roles of rainfall and temperature as climate change indicators for *B. napus* (Vernon, 2006). Despite being predominantly grown in high rainfall areas with long growing seasons, *B. napus* has shown adaptability to low rainfall zones through the release of short season cultivars (Si and Walton, 2004). This geographical and seasonal adaptation highlights *B. napus* as an exceptional model crop for studying phenotypic plasticity and applications to adaptation strategies. Seed oil content (SOC) is a crucial trait in *B. napus*, influenced by both genetic and environmental factors (Tan et al., 2022, Tan et al., 2011, Baud and Lepiniec, 2010, Gunasekera et al., 2006, Han et al., 2022). Previous studies have suggested that SOC of *B. napus* can be improved via traditional breeding and biotechnological approaches. However, integrative approaches that maximize SOC under future climate variability are lacking.

Here, we investigated the environmental indices and genetic basis behind phenotypic plasticity and propose an approach to facilitate crop breeding and agronomic practices in the face of climate change. In contrast to previous studies of phenotypic plasticity, we harnessed phenotypic plasticity to select optimal planting dates and identify adaptive genotypes to achieve the highest SOC for current and future environmental conditions. To this end, we used a diversity panel of 505 *B. napus* inbred lines and conducted multi-environment trials in sites with contrasting weather patterns. Our study presents a systematic framework for determining the factors contributing to phenotypic plasticity, which can help to prepare for the consequences of climate change on agriculture.

Results

Genotype-by-environment interaction for SOC

We conducted multi-environment trials with a diversity panel of 505 *B. napus* lines to examine the effect of genotype-by-environment interaction (G×E) on SOC. We carried out these trials at three different sites (Chengdu, CD; Wuhan, WH, and Hefei, HF), spanning a wide geographical range with diverse temperature and precipitation patterns (Fig. 1a, b; Supplementary Tables S1, S2). To account for potential year-to-year variations in temperature and precipitation, we conducted these trials for up to 4 years at each site. We assessed the contributions of genotype and environment to the observed variation in SOC in the multi-environment trials. SOC values among all *B. napus* lines show Pearson’s correlation coefficients from 0.27 to 0.68 across eight environments, indicating the influence of the environment on SOC (Fig. S1a, b). Looking at the influence of genotype, we obtained correlation coefficient values from -0.87 to 0.99 for all pairs of inbred lines (Fig. S1c). An analysis of variance for SOC across all eight environments indicates that environment, genotype, and G×E have similar contributions, explaining 23.75%, 25.26%, and 18.90% of the SOC variation, respectively (Supplementary Tables S5, S6). Thus, genotype and environment both influence SOC in this population.

We then analyzed the phenotypic variation in SOC using a joint regression analysis. For each genotype, we captured SOC across eight environments by a linear regression model with two parameters: the intercept, which represents the average response of a given genotype to the eight environments, and the slope, which represents the plasticity of that genotype to different environments (Fig. 1c). The resulting models show

a strong correspondence with the SOC observations, as indicated by the goodness-of-fit ($R^2 = 0.56$, on average). We observed substantial variation in both the intercept (ranging from 39.44% to 46.62% oil) and the slope (ranging from -0.59 to 2.36) among different genotypes. To investigate whether these variations are influenced by population structure, we divided our *B. napus* lines into five subgroups based on genome-wide single nucleotide polymorphisms (SNPs) and examined SOC variation within each subgroup. We observed no effect from population structure on intercept or slope, with little correlation between these two parameters in either the overall population ($r = 0.01$) or individual subgroups ($r = 0.01$ – 0.24 , Fig. S2). This finding suggests that genotypes with higher or lower average responses to all eight environments do not necessarily exhibit higher or lower plasticity to different environments.

We further investigated crossover occurrence by analyzing the proportion of pairs of lines experiencing changes in ranking, a prominent type of GxE (Xiong et al., 2021). Crossover occurrence is not evenly distributed across environmental means, with the highest occurrence observed near the center of the distribution (Fig. 1d). To examine whether this distribution is associated with variable genetic architecture across environments, we assessed the SNP-based heritability, which quantifies the proportion of phenotypic variation attributed to genetic variation. SNP-based heritability varies among environments, ranging from 0.13 to 0.56, and tends to be lower in environments closer to the center of the environmental mean (Supplementary Table S7). These estimations reveal that the variable genetic architectures across environments explain the GxE effects observed in this *B. napus* population.

Identification of environmental indices that influence SOC plasticity

To define the environmental factors influencing SOC, we examined the general trends of three key climate conditions during the growth season: temperature, precipitation, and solar radiation. Among the three experimental sites, Hefei (HF) exhibits the lowest cumulative growing-degree day (GDD) values, while Chengdu (CD) has the least amount of cumulative precipitation (Fig. 1b; Fig. S3). For solar radiation, Wuhan (WH) has higher levels of ultraviolet B (UV-B) irradiation during the leaf stage than the other sites. However, this trend diminishes and eventually reverses as the plants progress to inflorescence emergence and later stages (Fig. S4). In addition, variations in environmental conditions between different years at the same site also contributed to SOC plasticity (Fig. 1b, Fig. S3, S4). We identified days of cold stress (below -3.0degC) as a significant variable, with a noticeable disparity between years, with 33 days in HF2018 and 17 days in HF2017, suggesting that low temperature should be considered when assessing SOC differences (Fig. S3). These climate conditions are likely to be pivotal factors influencing SOC plasticity, but further investigation is needed to determine the key phases that affect SOC performance more explicitly.

To identify the explicit environmental indices that contribute to SOC plasticity, we used the CERIS package, a tool designed for analyzing phenotypic plasticity (Fig. S5). Through the exploration of various combinations of environmental parameters and growth windows, CERIS identified three factors: $\text{DTR}_{183-192}$, $\text{PR}_{166-195}$, and $\text{UVB}_{144-186}$, showing strong correlation with environmental means, thus determining SOC plasticity in eight different environments (Fig. 2). $\text{DTR}_{183-192}$ represents the average diurnal temperature range within the window of 183–192 days after planting. This window falls within the pod-filling stage, highlighting plant sensitivity to temperature changes during this stage. $\text{PR}_{166-195}$ and $\text{UVB}_{144-186}$ represent the average precipitation (PR) and average UV-B irradiation (UVB) in the windows of 166–195 and 144–186 days after planting, respectively. These two windows coincide with the flowering and pod-filling stages. To quantify the influence of these environmental indices on SOC, we conducted separate regressions of the environmental mean for SOC with each factor, revealing a 0.78% decrease in SOC for every 1-unit increment in $\text{DTR}_{183-192}$, a 1.55% increase in $\text{PR}_{166-195}$, and a 1.9% decrease in $\text{UVB}_{144-186}$ (Fig. S6). These findings establish a quantitative link between environmental indices, growth stages, and SOC plasticity, thereby enhancing our understanding of the environmental basis of SOC plasticity.

Identifying optimal planting dates and empirical validation

To maximize crop productivity by harnessing phenotypic plasticity, we propose a strategic approach for selecting the most advantageous planting dates. Indeed, the timing of planting influences the weather

conditions experienced by the crop during crucial growth stages. To identify the optimal planting dates at the three tested sites in this study (Fig. 3a), we predicted SOC for several new planting dates with the regression model of SOC on the identified environmental indices ($DTR_{183-192}$, $PR_{166-195}$ and $UVB_{144-186}$), conditioned on the assumption of a linear reaction norm pattern across the environments (see Methods). To ensure a practical planting guide, we limited the dates to within 10 days before or after the actual planting dates. We then compared the measured SOC at actual planting dates to the predicted SOC values for early or late plantings. We determined that planting 10 days earlier would have resulted in higher SOC, while planting 10 days later would have decreased SOC (Fig. 3b; Supplementary Table S8). Specifically, early planting resulted in an increase of up to 13.80% (HF2018), whereas late planting caused a decrease of up to 8.92% in SOC (WH2018).

To assess the general applicability of our approach for selecting optimal planting dates, we predicted SOC at four additional sites not included in the initial testing. We chose these sites from major oilseed producing areas in China (Fig. 3a; Supplementary Table S9). Using historical weather data from 2011 to 2020, we calculated the predicted SOC for each planting date between September 10th and October 28th at all seven sites (Fig. 3c). Early planting also generally leads to higher SOC compared to late planting, even for the four sites from which we lacked experimental data. The SOC varies among the seven planting sites at the optimal and earliest planting dates, with the highest SOC observed at CS (48.9%) and the lowest at CD (38.65%). In addition, the decrease in SOC is more pronounced at high altitude sites (e.g., ZZ) compared to low altitude sites (e.g., CS) when planting is not conducted at or near the optimal date (Supplementary Table S10).

We conducted empirical validation of the above SOC predictions with three planting dates in two new environments. We chose 50 lines from the diversity panel and planted them in Wuhan (WH2023) and Ezhou (EZ2023) on three different dates separated by 10 days each time. Generally, we observed that late planting results in lower SOC in both environments. We also predicted the SOC performance of all 50 inbred lines during the 2023 season using environmental data from the three identified indices ($DTR_{183-192}$, $PR_{166-195}$ and $UVB_{144-186}$). We obtained high prediction accuracies at both locations, with Pearson’s correlation coefficients of 0.62 and 0.67 in WH2023 and EZ2023, respectively (Fig. 4).

Identifying genes that determine SOC plasticity

To uncover the genetic basis of SOC plasticity, we conducted genome-wide association studies (GWASs) using two reaction norm parameters as phenotypic input, the intercept and the slope, obtained from joint regression analysis based on the environmental mean for SOC across all environments (Fig. S7). When using the intercept as the phenotype, we detected genomic regions containing the *PROBABLE METHYLTRANSFERASE PMT6* (*PMT6*) and *DIOXYGENASE FOR AUXIN OXIDATION1* (*DAO1*) genes, with *PMT6* previously reported to influence SOC variation in *B. napus* (Tang et al., 2021). Using the slope as phenotype, we identified two genomic regions containing genes homologous to *Arabidopsis* (*Arabidopsis thaliana*) *MYB DOMAIN PROTEIN 106* (*MYB106*) and *DIGALACTOSYL DIACYLGLYCEROL DEFICIENT1* (*DGD1*). *MYB106* encodes a MIXTA-like transcription factor involved in cuticle development and lipid transport, while *DGD1* encodes a galactosyltransferase-like protein involved in lipid trafficking (Dormann et al., 1999, Oshima et al., 2013).

To uncover the genomic regions that respond to changes in the identified environmental indices ($DTR_{183-192}$, $PR_{166-195}$ and $UVB_{144-186}$), we calculated the slope from a regression between SOC and each index, representing the specific response of each plant to each index. We used the resulting slopes as phenotypes for the GWAS (Figs. 5a, S8). We identified *DGD1* for $DTR_{183-192}$ slopes and *MYB106* for $UVB_{144-186}$ slopes. We also mapped three additional genomic regions associated with $PR_{166-195}$ slopes. We prioritized the candidate genes within these regions with the *Arabidopsis* homologs *3-HYDROXYACYL-[ACYL-CARRIER-PROTEIN] DEHYDRATASE* (*HAD*), *MYO-INOSITOL-1-PHOSPHATE SYNTHASE3* (*MIPS3*), and *PHOSPHATIDYLSERINE DECARBOXYLASE1* (*PSD1*). *HAD* is a 3-hydroxyacyl-ACP dehydratase involved in fatty acid biosynthesis. *MIPS3* catalyzes the rate-limiting step in myo-inositol biosynthesis. *PSD1* is a mitochondrion-localized protein involved in phosphatidylethanolamine biosynthesis (Fig. 5a–c). The

involvement of these genes in lipid metabolism in *Arabidopsis* is consistent with their putative role in SOC variation in *B. napus*.

To delineate potential polymorphisms in the above candidate genes, we aligned their genomic sequences from eight publicly available whole-genome assemblies of *B. napus* lines (Fig S9; Supplementary Table S16). We discovered structural variations in *PMT6* and *DGD1*, in the form of transposon insertions in their promoters, defining two haplotypes among these eight *B. napus* inbred lines. *PMT6* in ‘Gangan’, ‘QuintaA’ and ‘Shengli’ contains an insertion of a *Mutator* retrotransposon; *Helitron* retrotransposon was inserted in the *DGD1* promoter in ‘Shengli’. *PMT6* and *DGD1* may therefore affect SOC through changes in their expression levels. We also investigated potential coding variants affecting protein function. The most significant amino acid polymorphisms are C106G, H32N and S108C in DAO1, MYB106 and HAD, respectively. These variants provide relevant evidence for follow-up studies of functional polymorphisms.

To understand gene–environment interactions, we examined genetic effect dynamics along the identified environmental indices. We calculated the genetic effects within each environment for the most significant markers within identified candidate genes and used regression analysis to obtain fitted lines representing the genetic effects along the environmental gradient (Fig. 5d–f). This helps interpret the underlying mechanism of plant perceptor interacting with diverse environmental and development cues. Differential sensitivity (DS; magnitude change), conditional neutrality (CN, effect limiting to specific environment), antagonistic pleiotropy (AP; sign change), and no GxE (no change) (Des Marais et al., 2013) can be viewed as emergent properties in systems. When *DGD1* interacts with DTR₁₈₃₋₁₉₂, 57.14% of effect pairs show AP, with 35.71% showing DS and 7.14% indicating no GxE (Fig. 5d). The *MYB106* and UVB₁₄₄₋₁₈₆ interaction is predominantly AP (42.86%), followed by 25.00% CN, 21.43% DS, and 10.71% no GxE (Fig. 5f). In contrast, the *HAD* and PR₁₆₆₋₁₉₅ interaction is primarily CN (39.29%), followed by 32.14% AP, 21.43% DS, and 7.14% no GxE (Fig. 5e). We asked if the two alleles at each SOC plasticity gene showed differences in their expression levels; to this end, we used RNA sequencing data from 289 lines of developing seeds at 20 days after flowering in WH2016 (Tang et al., 2021). Indeed, the two possible alleles differed significantly in their expression, supporting a role in SOC plasticity (Figs. 5g–i, S10).

Identifying optimal haplotypes for future climates

To ensure adaptation to future climates, exploiting genetic variation for phenotypic plasticity is crucial. To identify genotypes suitable for various planting sites with different possible future climates, we examined the plasticity of SOC as a function of the genotype at the candidate plasticity genes in the eight environments. Here, we used PR₁₆₆₋₁₉₅ as a critical environmental index due to data unavailability and the absence of noticeable change in the other two indices (Fig S11). We observed changes in the ranking of gene–environment interactions for all candidate genes (*MYB106*, *MIPS3*, *HAD*, *DGD1* and *PSD1*) in response to PR₁₆₆₋₁₉₅ (Fig S12). To achieve high SOC, the allele with greater plasticity (as defined by higher slope) should be preferred in environments with higher precipitation, while the allele with lower plasticity should be favored in environments with lower precipitation.

We further examined SOC plasticity when considering the two possible alleles for all five candidate plasticity genes. From the 32 possible haplotypes, we focused on the 10 most abundant among the 505 *B. napus* lines and calculated the reaction norms for each haplotype in response to the environmental index PR₁₆₆₋₁₉₅. We observed varied plasticity levels among the 10 major haplotypes (Fig. 6a, b). Haplotype 1 (with the allele combination AAGTA for *MYB106*, *MIPS3*, *HAD*, *DGD1* and *PSD1*), consisting of 329 lines and representing 65% of the entire population, displays the lowest plasticity, as illustrated by the lowest slope of its regression with PR₁₆₆₋₁₉₅. It performs well in environments with lower precipitation but lags behind in environments with higher precipitation. By contrast, Haplotype 10 (allele combination CGAAA), composed of only five lines, presents the highest plasticity. It significantly outperforms the other haplotypes in terms of SOC, particularly in response to extremely high precipitation. This comparison suggests that most of the preserved germplasm has the potential to thrive in relatively dry environments, based on their SOC. However, we have a limited number of germplasms with rare haplotypes that are well suited to wet environments.

To develop varieties for future climates, we initially examined the precipitation patterns in major oilseed producing areas. We collected PR_{166–195} data from seven planting sites, including tested and untested sites, from 1960 to 2080. Based on this data, we identified three distinct categories of precipitation conditions. The first category comprises the sites CD and ZZ, with an average precipitation of 1.0 mm per day with no significant change over time. The second category includes the sites WH, HF and NJ, with average precipitation increasing from 2.0 to 3.9 mm per day throughout the years. The third category involves the sites CS and NC, experiencing an increase in precipitation from 5.0 to 7.7 mm per day on average (Fig. 6c). We then determined the optimal haplotype with the highest SOC for the past and future PR_{166–195} level at each site. In drier regions (CD and ZZ), haplotype 5 consistently demonstrated the highest SOC in both past and future scenarios. For more humid areas (WH, HF and NJ), haplotype 2 was the best performer in the past but is predicted to be replaced by haplotype 10 in future climates. In high-humidity regions (CS and NC), haplotype 10 was beneficial in both the past and future scenarios (Fig. 6d). Increasing the prevalence of haplotype 10 in future germplasms could be a viable approach to developing varieties that are well adapted to future climates.

Discussion

Analyzing phenotypic plasticity for climate-adapted practices

Adapting agricultural systems to climate change involves implementing changes in agronomic practices or cultivar selection to ensure successful crop cultivation in altered environmental conditions (Sloat et al., 2020). To achieve these changes, it is important to understand the gene x environment interaction and how it affects crop performance. Equally important is translating this mechanistic understanding into practical solutions for agronomic practices or cultivar selection (Bailey-Serres et al., 2019). This study focuses on analyzing phenotypic plasticity to identify environmental indices, genes and their modes of action. We then used this information to predict ideal planting dates for various environmental conditions and determine the optimal haplotypes for future climates. In the case of *B. napus*, a key trait is SOC. We identified three environmental indices (DTR_{183–192}, PR_{166–195} and UVB_{144–186}) and five responsive genes (*MYB106*, *HAD*, *MIPS3*, *DGD1* and *PSD1*) that influence SOC. Using this information, we predicted the SOC for various planting dates and validated these predictions in two new environments. By considering the plasticity of allele combinations from the five identified genes, we determined an optimal haplotype for each production site, which demonstrates the ability to adapt to future climate projections. The identification of production-limiting factors and the development of strategies for agricultural adaptation to climate change are essential for mitigating concerns regarding food security (Mourtzinis et al., 2019).

Three environmental indices determine SOC

Unlike previous research, which focused on identifying a single environmental factor to represent environmental mean in studies of phenotypic plasticity (Li et al., 2018, Guo et al., 2020), we uncovered three environmental factors as fundamental to plant growth and development. The inclusion of multiple factors is advantageous for capturing the complex and multifaceted nature of the genotype–environment–phenotype relationship, while also enhancing the accuracy of predicting traits in new environments (Millet et al., 2019). Although these factors are closely related, we did not consider the issue of multicollinearity in this study due to our emphasis on prediction, but it should be taken into account when determining the significance of these factors (Kim, 2019). We demonstrated that environmental factors have various influences on the final phenotype at different developmental phases, particularly the growth windows of 183–192, 166–195 and 144–186 days after planting, which align with the flowering or pod-filling stages of *B. napus*. It would be ideal to identify specific environmental indices for each genotype (Sabir et al., 2023), but a more practical approach should use a harmonized index shared by all genotypes for prediction and application purposes.

Identification of slope genes that differ from intercept genes

The genetic basis of SOC variation in *B. napus* has been deciphered through genome- and transcriptome-wide association studies, leading to the identification of numerous genomic regions and/or genes associated with this trait (Tang et al., 2021). In our study, we identified the same set of significant genomic regions when

using intercept as the phenotype. Notably, when we used slope as the phenotype and conducted GWAS, we discovered five genes homologous to the *Arabidopsis* genes *MYB106*, *MIPS3*, *HAD*, *DGD1* and *PSD1* known to be involved in oil metabolism. Moreover, these genes interact with the identified environmental indices and exhibits dynamic effects in response to changes in these indices. The findings highlight the complex interplay between genes and the environment and offer new insights into the genetic basis of SOC variation from the perspective of phenotypic plasticity.

Predicting optimal planting dates and haplotypes in multiple environments

Finding the optimal planting dates can significantly increase growth, development and crop production (Baum et al., 2019). Nevertheless, this undertaking poses difficulties due to various modulating factors (Sacks et al., 2010). While local agricultural facilities often provide recommendations based on historical records, these suggestions are not always reliable. To tackle this issue, our study used the reaction norm to quantify the phenotypic plasticity of each genotype and predicted trait performance based on weather conditions specific to each planting date and location, from which we proposed the optimal planting date. In the future, our approach can be further improved by incorporating crop models that incorporate a physiological description of crop growth using advanced mathematical algorithms (Hammer et al., 2005). This integration will enhance our ability to explain and predict crop growth and development, while also simplifying the extensive parameter calibration work required by crop models, especially for large-scale and long-term simulations.

Based on an analysis of phenotypic plasticity into the interactions between genes and environmental indices, we generated a prediction model for the relationship between trait performance and these interactions. Using this model, we evaluated the genetic potential of different genotypes to adapt to future climates. We used a precipitation-related environmental index to estimate projected future climate conditions. Other environmental factors, like irradiation, soil moisture and nitrogen application, may emerge as critical in other scenarios, and we may be able to model nonlinear relationships among them (Scheres and van der Putten, 2017, Hammer et al., 2010). While our study used projected future climates for trait performance prediction, it is essential to acknowledge that the accuracy of these predictions may require improvement as more precise estimates of climate change become available. With the aid of powerful tools in artificial intelligence and biotechnologies, advanced models are currently being developed to enhance the precision of breeding and agronomy practices in response to a changing climate. By building upon the establishment of mechanistic links and advanced models, we can effectively address fundamental questions related to phenotypic plasticity and develop potential breeding and agronomic strategies.

Materials and Methods

Population and phenotyping

A diversity panel of 505 *B. napus* accessions was grown in three different sites: Wuhan (WH; 114deg 21'E, 30deg 28'N) for 4 years (2015–2016, 2016–2017, 2017–2018 and 2018–2019), Hefei (HF; 117deg 13'E, 31deg 52'N) for 2 years (2016–2017 and 2017–2018) and Chengdu (CD; 104deg 12'E, 30deg 46'N) for 2 years (2016–2017 and 2019–2020). Additionally, a subset of 50 accessions, consisting of 25 high-plasticity lines and 25 low-plasticity lines, was grown in Wuhan and Ezhou (EZ; 114deg 42'E, 30deg 21'N) on three different planting dates in 2022. In Wuhan, the planting dates were September 27th, October 7th, and October 17th (WH1, WH2 and WH3); in Ezhou, the dates were October 8th, October 18th, and October 28th (EZ1, EZ2 and EZ3). The phenotypic data for WH2016, WH2017, WH2018, HF2017, HF2018 and CD2017 were obtained from a previous study (Tang et al., 2021). Mature open-pollinated seeds of the natural population were harvested and dried for SOC analysis with a Foss NIRSystems 5000 near-infrared reflectance spectroscope (Li et al., 2003). Six biological replicates per accession were used for analysis. Detailed phenotype and genotype data can be found in supplemental files (Supplementary Tables S3, S4) or in the previous study (Tang et al., 2021).

Analysis of variance and estimation of variance components

The phenotypic value for genotype i when tested in replicate k in the environment j was modeled as $y_{ijk} = u + g_i + t_j + b_{k(j)} + (gt)_{ij} + e_{ijk}$, where u is the population mean, g_i is the effect of genotype i , t_j is the effect of environment j , $b_{k(j)}$ is the block effect associated with replicate k nested in the environment j , $(gt)_{ij}$ is the G x E effect associated with genotype i and environment j and e_{ijk} is the error.

The analysis of variance was conducted using the R function “aov” that fits a model with the function “lm” for each stratum. The estimation of variance components was conducted with the R package “VCA” and the function “anovaVCA.”

Population structure analysis and SNP-based heritability estimation

A quality control analysis was conducted on the materials using Plink (Purcell et al., 2007). Initially, SNPs with a minor allele frequency (MAF) < 0.05 were removed. Subsequently, materials with SNP missing rates > 0.1 were excluded. Finally, after filtering the original SNPs (Tang et al., 2021), a final set of 8,503,071 SNPs was obtained, with a median MAF of 0.21. In addition, Plink was used to calculate the genomic relationship matrix (GRM) among the 505 accessions. Principal component analysis (PCA) was then performed based on this matrix. In the resulting PCA plot, the accessions were differentiated into subgroups reflecting their ecological types. Our materials included five ecological types: semi-winter 1 (SW1), semi-winter 2 (SW2), semi-winter mixed (SWM), spring (SPR) and mixed.

Using the GRM above, the SNP-based heritability was calculated with SOC as the phenotype. This analysis was conducted for each environment using GCTA (Yang et al., 2011), with the recommended parameters ‘-bfile -make-grm -make-grm-ald 0 -out; -grm -pheno -reml -out’.

Identifying the environmental index

Environmental data were retrieved from the websites of the National Oceanic and Atmospheric Administration (NOAA: <https://www.noaa.gov/weather>) and the Astronomical Applications Department of the US Naval Observatory (<https://www.usno.navy.mil/USNO/astronomical-applications>). Daily temperatures (degF) were converted to growing-degree days (GDDs) for *B. napus* with the formula: $GDD = [(maximum\ temperature + minimum\ temperature) / 2] - 37.4$ (Marshall and Squire, 1996, Pullens et al., 2019). The daily diurnal temperature range (DTR) was calculated as $T_{max} - T_{min}$. Phenotypic data were collected from 505 *B. napus* inbred lines planted in eight environments (Supplementary Table S3), along with environmental data (Supplementary Table S11) covering the entire growth period in these eight environments. Three categories of environmental parameters were tested: temperature (GDD and DTR), moisture (precipitation [PR] and relative humidity [RH]) and light (clear sky photosynthetically active radiation [CPAR] and ultraviolet B [UVB]) by implementing the CERIS algorithm in R to identify environmental indices (https://github.com/jmyu/CERIS_JGRA) (Li et al., 2018). The most relevant environmental index in the three categories of environmental parameters for SOC was separately chosen according to the highest correlation between environmental means and environmental index within the corresponding search window (Figs. 2b, S5).

Phenotypic prediction at different locations and periods

After environmental indices were identified, they were leveraged to predict phenotypic outcomes in different environments (Guo et al., 2020, Li et al., 2022, Li et al., 2021). Here we identified three environmental indices. For any environmental index, we employed the same approach in constructing the model. Firstly, one model was constructed to estimate the magnitude of changes in phenotypic response to each environmental index at the population level by a general linear model (Fig. S6):

$$y_i = \beta_0 + \beta_1 x_i + \epsilon_i$$

where y_i is the mean SOC for the population in the i th environment ($i = 1, 2 \dots v$), x_i is the mean values for the environmental index in the i th environment, β_0 is the intercept of the linear model, ϵ_i is the deviation from regression and β_1 is the slope estimate of the linear model, which indicated the expected trait value

change per a one-unit change of the corresponding climatic variant (Li et al., 2022). Subsequently, the other two models are also constructed using the same theoretical framework. Finally, environmental data were retrieved for each location and for each simulated planting date, extracting three environmental indices corresponding to that environment. Subsequently, values of these environmental indices were used as input into separate models, the averaged output values of the three models were calculated, ultimately yielding the predicted phenotypic value.

To predict the SOC when planting 10 days earlier or later than the designated planting period in the established cultivation area and ensure prediction stability, following the above approach, the predicted outcomes computed for planting 9 days early, 10 days early and 11 days early were averaged as the prediction for planting 10 days early. Similarly, the predicted outcomes for planting 9 days late, 10 days late and 11 days late were averaged as the prediction for planting 10 days late (Fig. 3b; Supplementary Table S11). For predicting the trend of SOC variation as a function of planting dates in seven primary *B. napus* producing regions in the middle and lower Yangtze River, environmental data were obtained for 10 years (2011–2020) (Supplementary Table S13). Daily SOC predictions were conducted from September 10th to October 28th, using the environmental data accumulated over the preceding decade for the prediction on each day (Fig. 3c).

Empirical validation

After the completion of the initial analysis and model building, empirical validation experiments were carried out. Specifically, a subset of 50 inbred lines, consisting of 25 high-plasticity lines and 25 low-plasticity lines, was grown in Wuhan (114° 21'E, 30deg 28'N) and Ezhou (114deg 42'E, 30deg 21'N) on three different planting dates in 2022 (Supplementary Table S4). For any environmental index, we employed the same approach in constructing the model. First, one model was constructed to estimate the magnitude of changes in phenotypic response to each environmental index at the individual level by joint regression analysis (Guo et al., 2023) (Fig. S9; Supplementary Table S3):

$$Y_{ij} = u_i + \beta_i I_j + \delta_{ij}$$

where Y_{ij} is the line mean of the i th line in the j th environment ($i = 1, 2 \dots v; j = 1, 2 \dots n$); u_i is the mean of the i th line across all environments; β_i is the regression coefficient that measures the response of the i th line to environmental input; I_j is the environmental mean, expressed as the mean of all lines in the j th environment; and δ_{ij} is the deviation from regression. After that, the other two models are also constructed using the same theoretical framework. Subsequently, environmental data were collected from NOAA and USNO (Supplementary Table S14) and separately used as input for these three models to predict the SOC of the 50 lines. The final predicted value for each line was the average output from these three models. Finally, the accuracy of the model was evaluated by examining the correlation between the predicted and observed values of each inbred line, measured as Pearson's correlation coefficients (Fig 4b, c).

Genome-wide association study (GWAS) and linkage disequilibrium

Reaction norms connect the environments to which a particular genotype is exposed and the phenotypes produced by that genotype in these environments. From the reaction norm values, two reaction norm-norm parameters (intercept and slope) were obtained for each trait using a joint regression analysis of the observed trait values across environments (Fig. 1c). In addition, with the identified environmental indices, the slope was obtained for each index using a joint regression analysis of the observed trait values across environments (Fig. S9). Treating the estimates of intercept and slope as a derived trait, an established mixed-model GWAS (Zhang et al., 2010, Yu et al., 2006) implemented in GAPIT (v.3) R package (<http://zzlab.net/GAPIT>) (Wang and Zhang, 2021) was used, separately for each trait, to identify genomic regions underlying the observed variation for slope and intercept across different genotypes.

The significance thresholds of association were calculated with Genetic type I error calculator (GEC) software (Li et al., 2012), and the calculated significance threshold was 7.77×10^{-7} . To identify candidate genes, genes

within the 100-kb upstream and downstream regions of significant SNPs were extracted, according to the linkage disequilibrium (LD) decay rate estimated by previous studies (Tang et al., 2021).

Identification of candidate genes associated with phenotypic plasticity through GWAS

Within the LD interval upstream and downstream of the significant SNPs detected by GWAS, the *B. napus* homologs for seven candidate genes known to participate in the lipid metabolism of *Ara-bidopsis* seeds (<http://aralip.plantbiology.msu.edu/>) were detected: *PMT6* (BnaA05G0437100ZS), *DAO1* (BnaA09G0636200ZS), *MYB106* (BnaA01G0418000ZS), *HAD* (BnaC02G0039300ZS), *MIPS3* (BnaC02G0039400ZS), *DGD1* (BnaC05G0484900ZS) and *PSD1* (BnaC09G0366500ZS).

To investigate the variation in the promoter regions of these genes, the methodology described by Li was followed (Li et al., 2021). In detail, sequences surrounding the genes (*PMT6* and *DGD1*) implicated in SOC phenotypic plasticity were retrieved from the *B. napus* pan-genome information resource (BnPIR; <http://cbl.hzau.edu.cn/bnapus/>) for the inbred lines ZS11, Zheyu7, Gangan, Shengli, No2127, Westar, Quinta and Tapidor. The sequences of these two genes were also extracted from this website. The co-linear sequences among these eight inbred lines were used as queries for a BLAST search against each other to identify structural variations. Transposon elements (TEs) present in the sequences were identified with a TE Library constructed by Extensive de-novo TE Annotator (EDTA) (Ou et al., 2019). In addition, sequence variation within the genes (*DAO1*, *MYB106* and *HAD*) was analyzed with polyphen-2 (<http://genetics.bwh.harvard.edu/pph2/>) and provean (<http://provean.jcvi.org/>), noting putative loss-of-function alleles for each gene as predicted by at least one of the software platforms (Supplementary Table S16).

To model the genetic effect dynamics along the environmental gradient, SNPs significantly associated with slope were tested for association with SOC within each environment using the mixed-model method in GAPIT. These separate genetic effects were then regressed on the environmental gradients to generate the fitted lines as the genetic effect continua, defined as varied genetic effects with different environmental inputs (Fig. 5D-F).

We used RNA sequencing data from 289 lines (subset of 505 lines) of developing seeds at 20 days after flowering in WH2016 (Tang et al., 2021). The expression levels of the plasticity genes were determined by the abundance of transcripts and compared between two alleles with a Wilcoxon test.

Reaction norms at the single-locus and multi-locus combination level

After GWAS and candidate gene examination, the significant SNPs for PR₁₆₆₋₁₉₅ were used. Five SNPs were selected, with each SNP showing the most significant association with SOC plasticity and closely linked to each candidate gene (Fig. 5b).

The entire population was divided into two groups based on their homozygous genotype at each selected SNP, resulting in the AA and BB groups. In an individual environment, the genotypic value for AA (or BB) was the average phenotypic value across all individuals carrying the AA (or BB) genotype at the locus. Two lines were drawn in the reaction norm graph, one for each group (Fig. S12). Linear regression was applied to show the relationship between the genotypic value and the environment and to show the fitted genotypic values across all environments (Fig. S12).

The five SNPs result in $2^5 = 32$ possible haplotypes, with homozygous genotypes at each SNP. Similar to the calculation of genotypic values for a single locus described above, the genotypic value for each haplotype was the average phenotypic value for all inbred lines harboring each haplotype. There were 10 main haplotypes considered here for each environment (haplotypes represented by fewer than five inbred lines were not considered). Linear regression was applied to show the relationship between genotypic value and the environment and to show the fitted genotypic values across all environments (Guo et al., 2020) (Figs. 6a,b).

Obtaining climate data and phenotypic predictions in the past and future

To predict the adaptation potential of haplotype materials for past and future planting, meteorological data were acquired with the R package “raster” and the function “getData” (Supplementary Table S15). The precipitation and temperature data from 1961 to 2018 were retrieved from the historical monthly weather data section in WorldClim (<https://worldclim.org/data/monthlywth.html>). The predicted precipitation and temperature data from 2021 to 2080 were retrieved from the Future climate data section in WorldClim (<https://worldclim.org/data/cmip6/cmip6climate.html>). A spatial resolution of 10 minutes was selected, with the data aggregated to align with the scales of NOAA and USNO data.

September 20th was set as the simulated planting date for future predictions. The 166–195 interval for the environmental index PR was chosen, corresponding to March 5th to April 3rd. Precipitation data were extracted from this interval. Similarly, the 183–192 interval for the environmental index DTR was chosen, corresponding to March 22nd to March 31st. From this interval, minimum (tn) and maximum (tx) temperature data were extracted, resulting in DTR being defined as: $DTR = tx - tn$.

However, original models were constructed using data from NOAA and USNO. WorldClim data are on another scale, which was converted to the scales of NOAA and USNO. Subsequently, precipitation data in March from both databases between 1999 and 2018 in the seven locations were collected separately and fitted using a general linear model, revealing a correlation of 0.97 between the two datasets. A model, $y = 1.107x + 0.052$, was established, where y represents the precipitation data from NOAA and USNO, while x represents the precipitation data from WorldClim. Using this equation, WorldClim data were calibrated to match the scales of NOAA and USNO for subsequent predictions.

The means for climate data spanning 20-year intervals in historical records were computed, resulting in three periods: 1961–1980, 1981–2000 and 2001–2018. Incorporating the three future periods 2021–2040, 2041–2060 and 2061–2080 resulted in six data periods for each location (Fig. 6C). To assess the performance of each haplotype under varying periods, the environmental data were incorporated into the established multi-locus model. Using a colored bar chart representation on a map, the haplotype with the highest SOC was displayed alongside its corresponding SOC value. Additionally, the gray bars in the bar chart depict the population mean (Fig. 6d).

Author contributions:

T.G., L.G., and J.Y. conceived and designed the project. L.Z., X.H., J.X., H.P., Y.S., Y.C., Z.Z. and X.L. conducted the experiments and analyzed the data. X.H. and L.G. provided the GWAS population and collected the SOC data. X.L. and J.Y. contributed analysis tools and provided suggestions. L.G and T.G. wrote the manuscript. All authors read and approved the final manuscript.

References

- BAILEY-SERRES, J., PARKER, J. E., AINSWORTH, E. A., OLDROYD, G. E. D. & SCHROEDER, J. I. 2019. Genetic strategies for improving crop yields. *Nature*, 575, 109-118.
- BAUD, S. & LEPINIEC, L. 2010. Physiological and developmental regulation of seed oil production. *Progress in lipid research*, 49, 235-249.
- BAUM, M., ARCHONTOULIS, S. & LICHT, M. 2019. Planting date, hybrid maturity, and weather effects on maize yield and crop stage. *Agronomy Journal*, 111, 303-313.
- BONAMOUR, S., CHEVIN, L. M., CHARMANTIER, A. & TEPLITSKY, C. 2019. Phenotypic plasticity in response to climate change: the importance of cue variation. *Philos Trans R Soc Lond B Biol Sci*, 374, 20180178.
- DES MARAIS, D. L., HERNANDEZ, K. M. & JUENGER, T. E. 2013. Genotype-by-environment interaction and plasticity: exploring genomic responses of plants to the abiotic environment. *Annual Review of Ecology, Evolution, and Systematics*, 44, 5-29.

- DORMANN, P., BALBO, I. & BENNING, C. 1999. Arabidopsis galactolipid biosynthesis and lipid trafficking mediated by DGD1. *Science*, 284, 2181-2184.
- FU, J., JIAN, Y., WANG, X., LI, L., CIAIS, P., ZSCHEISCHLER, J., WANG, Y., TANG, Y., MULLER, C., WEBBER, H., YANG, B., WU, Y., WANG, Q., CUI, X., HUANG, W., LIU, Y., ZHAO, P., PIAO, S. & ZHOU, F. 2023. Extreme rainfall reduces one-twelfth of China's rice yield over the last two decades. *Nat Food*.
- GUNASEKERA, C., MARTIN, L., SIDDIQUE, K. & WALTON, G. 2006. Genotype by environment interactions of Indian mustard (*Brassica juncea* L.) and canola (*B. napus* L.) in Mediterranean-type environments: 1. Crop growth and seed yield. *European Journal of Agronomy*, 25, 1-12.
- GUO, T., MU, Q., WANG, J., VANOUS, A. E., ONOGI, A., IWATA, H., LI, X. & YU, J. 2020. Dynamic effects of interacting genes underlying rice flowering-time phenotypic plasticity and global adaptation. *Genome Research*, 30, 673-683.
- GUO, T., WEI, J., LI, X. & YU, J. 2023. Environmental context of phenotypic plasticity in flowering time in sorghum and rice. *Journal of Experimental Botany*, erad398.
- HAMMER, G. L., CHAPMAN, S., VAN OOSTEROM, E. & PODLICH, D. W. 2005. Trait physiology and crop modelling as a framework to link phenotypic complexity to underlying genetic systems. *Australian Journal of Agricultural Research*, 56, 947-960.
- HAMMER, G. L., VAN OOSTEROM, E., MCLEAN, G., CHAPMAN, S. C., BROAD, I., HARLAND, P. & MUCHOW, R. C. 2010. Adapting APSIM to model the physiology and genetics of complex adaptive traits in field crops. *J Exp Bot*, 61, 2185-202.
- HAN, X., TANG, Q., XU, L., GUAN, Z., TU, J., YI, B., LIU, K., YAO, X., LU, S. & GUO, L. 2022. Genome-wide detection of genotype environment interactions for flowering time in *Brassica napus*. *Frontiers in Plant Science*, 13, 1065766.
- HICKEY, L. T., A, N. H., ROBINSON, H., JACKSON, S. A., LEAL-BERTIOLI, S. C. M., TESTER, M., GAO, C., GODWIN, I. D., HAYES, B. J. & WULFF, B. B. H. 2019. Breeding crops to feed 10 billion. *Nat Biotechnol*, 37, 744-754.
- KIM, J. H. 2019. Multicollinearity and misleading statistical results. *Korean J Anesthesiol*, 72, 558-569.
- KUSMEC, A., SRINIVASAN, S., NETTLETON, D. & SCHNABLE, P. S. 2017. Distinct genetic architectures for phenotype means and plasticities in *Zea mays*. *Nature Plants*, 3, 715-723.
- LESK, C., ANDERSON, W., RIGDEN, A., COAST, O., JaGERMEYR, J., MCDERMID, S., DAVIS, K. F. & KONAR, M. 2022. Compound heat and moisture extreme impacts on global crop yields under climate change. *Nature Reviews Earth & Environment*, 3, 872-889.
- LI, G., XIULI, S., LIANG, J., GAOQUAN, W., JIUWEI, X., ZELAN, W. & TINGDONG, F. 2003. Establishment of math models of NIRS analysis for oil and protein contents in seed of *Brassica napus*. *Zhongguo Nong ye ke xue= Zhongguo Nongye Kexue*, 36, 1609-1613.
- LI, M.-X., YEUNG, J. M., CHERNY, S. S. & SHAM, P. C. 2012. Evaluating the effective numbers of independent tests and significant p-value thresholds in commercial genotyping arrays and public imputation reference datasets. *Human genetics*, 131, 747-756.
- LI, X., GUO, T., BAI, G., ZHANG, Z., SEE, D., MARSHALL, J., GARLAND-CAMPBELL, K. A. & YU, J. 2022. Genetics-inspired data-driven approaches explain and predict crop performance fluctuations attributed to changing climatic conditions. *Molecular Plant*, 15, 203-206.
- LI, X., GUO, T., MU, Q., LI, X. & YU, J. 2018. Genomic and environmental determinants and their interplay underlying phenotypic plasticity. *Proceedings of the National Academy of Sciences*, 115, 6679-6684.

- LI, X., GUO, T., WANG, J., BEKELE, W. A., SUKUMARAN, S., VANOUS, A. E., MCNELLIE, J. P., TIBBS-CORTES, L. E., LOPES, M. S. & LAMKEY, K. R. 2021. An integrated framework reinstating the environmental dimension for GWAS and genomic selection in crops. *Molecular Plant*,14, 874-887.
- LIU, N., DU, Y., WARBURTON, M. L., XIAO, Y. & YAN, J. 2020. Phenotypic Plasticity Contributes to Maize Adaptation and Heterosis. *Molecular Biology and Evolution* .
- MARSHALL, B. & SQUIRE, G. 1996. Non-linearity in rate-temperature relations of germination in oilseed rape. *Journal of Experimental Botany*, 47, 1369-1375.
- MILLET, E. J., KRUIJER, W., COUPEL-LEDRU, A., PRADO, S. A., CABRERA-BOSQUET, L., LACUBE, S., CHARCOSSET, A., WELCKER, C., VAN EEUWIJK, F. & TARDIEU, F. 2019. Genomic prediction of maize yield across European environmental conditions. *Nature genetics*,51, 952-956.
- MOURTZINIS, S., SPECHT, J. E. & CONLEY, S. P. 2019. Defining optimal soybean sowing dates across the US. *Scientific Reports*,9, 2800.
- MU, Q., GUO, T., LI, X. & YU, J. 2022. Phenotypic plasticity in plant height shaped by interaction between genetic loci and diurnal temperature range. *New Phytologist*, 233, 1768-1779.
- OSHIMA, Y., SHIKATA, M., KOYAMA, T., OHTSUBO, N., MITSUDA, N. & OHME-TAKAGI, M. 2013. MIXTA-like transcription factors and WAX INDUCER1/SHINE1 coordinately regulate cuticle development in Arabidopsis and Torenia fournieri. *The Plant Cell*, 25, 1609-1624.
- OU, S., SU, W., LIAO, Y., CHOUGULE, K., AGDA, J. R., HELLINGA, A. J., LUGO, C. S. B., ELLIOTT, T. A., WARE, D. & PETERSON, T. 2019. Benchmarking transposable element annotation methods for creation of a streamlined, comprehensive pipeline. *Genome biology*, 20,1-18.
- PIGLIUCCI, M., MURREN, C. J. & SCHLICHTING, C. D. 2006. Phenotypic plasticity and evolution by genetic assimilation. *J Exp Biol*,209, 2362-7.
- PULLENS, J. W. M., SHARIF, B., TRNKA, M., BALEK, J., SEMENOV, M. A. & OLESEN, J. E. 2019. Risk factors for European winter oilseed rape production under climate change. *Agricultural and Forest Meteorology*, 272, 30-39.
- PURCELL, S., NEALE, B., TODD-BROWN, K., THOMAS, L., FERREIRA, M. A., BENDER, D., MALLER, J., SKLAR, P., DE BAKKER, P. I. & DALY, M. J. 2007. PLINK: a tool set for whole-genome association and population-based linkage analyses. *The American journal of human genetics*,81, 559-575.
- SABIR, K., ROSE, T., WITTKOP, B., STAHL, A., SNOWDON, R. J., BALLVORA, A., FRIEDT, W., KAGE, H., LEON, J., ORDON, F., STUTZEL, H., ZETZSCHE, H. & CHEN, T. W. 2023. Stage-specific genotype-by-environment interactions determine yield components in wheat. *Nat Plants* .
- SACKS, W. J., DERYNG, D., FOLEY, J. A. & RAMANKUTTY, N. 2010. Crop planting dates: an analysis of global patterns. *Global ecology and biogeography*, 19, 607-620.
- SCHERES, B. & VAN DER PUTTEN, W. H. 2017. The plant perceptron connects environment to development. *Nature*, 543, 337-345.
- SI, P. & WALTON, G. H. 2004. Determinants of oil concentration and seed yield in canola and Indian mustard in the lower rainfall areas of Western Australia. *Australian Journal of Agricultural Research*,55, 367-377.
- SLOAT, L. L., DAVIS, S. J., GERBER, J. S., MOORE, F. C., RAY, D. K., WEST, P. C. & MUELLER, N. D. 2020. Climate adaptation by crop migration. *Nat Commun*, 11, 1243.
- TAN, H., YANG, X., ZHANG, F., ZHENG, X., QU, C., MU, J., FU, F., LI, J., GUAN, R., ZHANG, H., WANG, G. & ZUO, J. 2011. Enhanced seed oil production in canola by conditional expression of Brassica napus LEAFY COTYLEDON1 and LEC1-LIKE in developing seeds. *Plant Physiol*,156, 1577-88.

- TAN, Z., PENG, Y., XIONG, Y., XIONG, F., ZHANG, Y., GUO, N., TU, Z., ZONG, Z., WU, X., YE, J., XIA, C., ZHU, T., LIU, Y., LOU, H., LIU, D., LU, S., YAO, X., LIU, K., SNOWDON, R. J., GOLICZ, A. A., XIE, W., GUO, L. & ZHAO, H. 2022. Comprehensive transcriptional variability analysis reveals gene networks regulating seed oil content of *Brassica napus*. *Genome Biol*, 23, 233.
- TANG, S., ZHAO, H., LU, S., YU, L., ZHANG, G., ZHANG, Y., YANG, Q.-Y., ZHOU, Y., WANG, X. & MA, W. 2021. Genome-and transcriptome-wide association studies provide insights into the genetic basis of natural variation of seed oil content in *Brassica napus*. *Molecular Plant*, 14, 470-487.
- TIGCHELAAR, M., BATTISTI, D. S., NAYLOR, R. L. & RAY, D. K. 2018. Future warming increases probability of globally synchronized maize production shocks. *Proc Natl Acad Sci U S A*, 115, 6644-6649.
- VERNON, L. 2006. *Potential impacts of climate change on agricultural land use suitability : canola* / Luke Vernon and Dennis van Gool, [South Perth, W.A.], Dept. of Agriculture.
- WANG, J. & ZHANG, Z. 2021. GAPIT version 3: boosting power and accuracy for genomic association and prediction. *Genomics, proteomics & bioinformatics*, 19, 629-640.
- XIONG, W., REYNOLDS, M. P., CROSSA, J., SCHULTHESS, U., SONDER, K., MONTES, C., ADDIMANDO, N., SINGH, R. P., AMMAR, K., GERARD, B. & PAYNE, T. 2021. Increased ranking change in wheat breeding under climate change. *Nat Plants*, 7, 1207-1212.
- XUE, B. & LEIBLER, S. 2018. Benefits of phenotypic plasticity for population growth in varying environments. *Proc Natl Acad Sci U S A*, 115, 12745-12750.
- YANG, J., LEE, S. H., GODDARD, M. E. & VISSCHER, P. M. 2011. GCTA: a tool for genome-wide complex trait analysis. *The American Journal of Human Genetics*, 88, 76-82.
- YU, J., PRESSOIR, G., BRIGGS, W. H., VROH BI, I., YAMASAKI, M., DOEBLEY, J. F., MCMULLEN, M. D., GAUT, B. S., NIELSEN, D. M. & HOLLAND, J. B. 2006. A unified mixed-model method for association mapping that accounts for multiple levels of relatedness. *Nature genetics*, 38, 203-208.
- ZHANG, Z., ERSOZ, E., LAI, C.-Q., TODHUNTER, R. J., TIWARI, H. K., GORE, M. A., BRADBURY, P. J., YU, J., ARNETT, D. K. & ORDOVAS, J. M. 2010. Mixed linear model approach adapted for genome-wide association studies. *Nature genetics*, 42, 355-360.
- ZHAO, Z., WANG, E., KIRKEGAARD, J. A. & REBETZKE, G. J. 2022. Novel wheat varieties facilitate deep sowing to beat the heat of changing climates. *Nature Climate Change*, 12, 291-296.

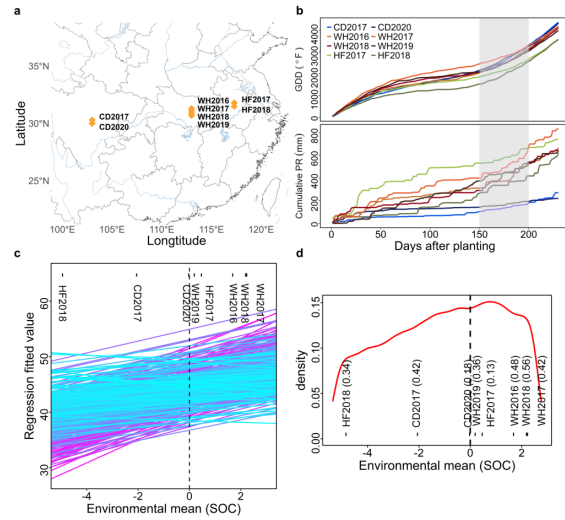


Fig. 1 Plasticity for seed oil content in a *Brassica napus* diversity panel across multi-environment trials. **a**, Map showing the eight natural field environments at three sites over up to 4 years. **b**, Cumulative temperature and precipitation profiles for the eight environments. Gray areas indicate the approximate flowering and pod filling stages. **c**, Reaction norms for seed oil content (SOC) in all inbred lines within the diversity panel. **d**, Crossover occurrence over environments. Environments closer to the center of the environmental mean exhibit higher crossovers (red line) and lower SNP-based heritability (numbers in parentheses). GDD, growing degree days; PR, precipitation. Three tested sites are Chengdu (CD), Wuhan (WH), and Hefei (HF).

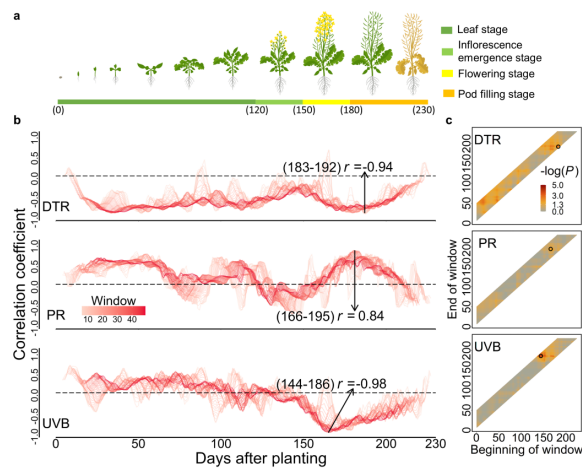


Fig. 2 Three environmental indices determine seed oil content plasticity in *Brassica napus*. **a**, Diagram of growth stages in *B. napus*. **b**, Correlations between the environmental mean and DTR, PR and UVB values throughout the growing season. DTR₁₈₃₋₁₉₂, PR₁₆₆₋₁₉₅ and UVB₁₄₄₋₁₈₆ show the most significant correlations with environmental mean. DTR, diurnal temperature range; PR, precipitation; UVB, ultraviolet B. Numbers in parentheses (on the plots) or in subscript for each environmental index indicate days after planting. **c**, Significance of correlation between the environmental mean and environmental indices within the search window.

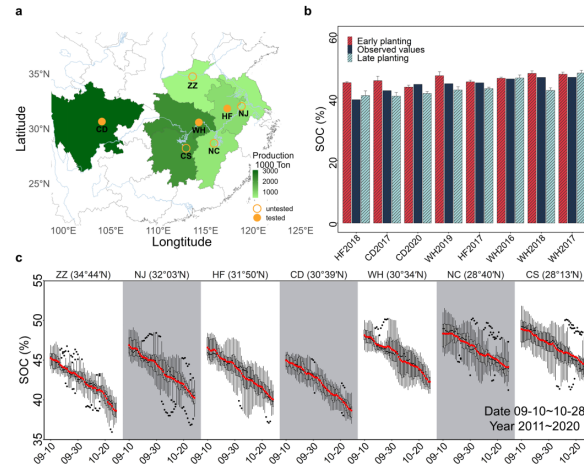


Fig. 3 Identifying optimal planting dates for high seed oil content in predominant *Brassica napus* production areas. **a**, Map showing average yields in major *B. napus* production areas, with three tested sites (filled circles) and four sites for prediction (open circles). **b**, SOC at different planting dates (10 days early, normal and 10 days late) in eight tested environments. **c**, Predicted SOC with different planting dates in both tested and untested sites. The black dots represent the predicted SOC from 2011 through 2020, while the red dots indicate the average values.

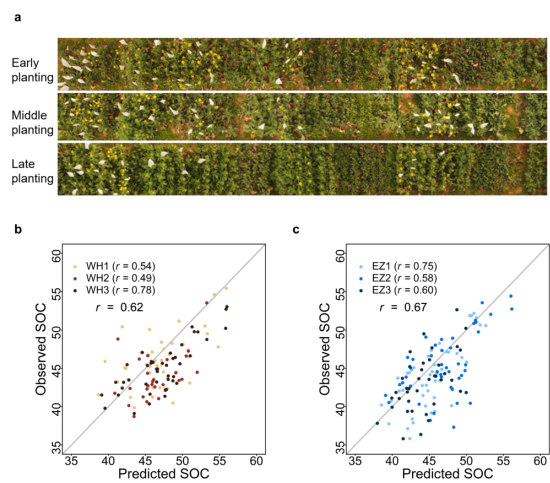


Fig. 4 Empirical validation of seed oil content predictions with three planting dates in two new environments. a, Aerial photographs of fields from WH2023 when *B. napus* lines were planted at three different dates. b–c, Scatterplots showing the correlation between the measured and predicted SOC values in the environments of WH2023 (b) and EZ2023 (c). The numbers of 1, 2 and 3 after location names (WH and EZ) indicate early, middle and late planting, respectively.

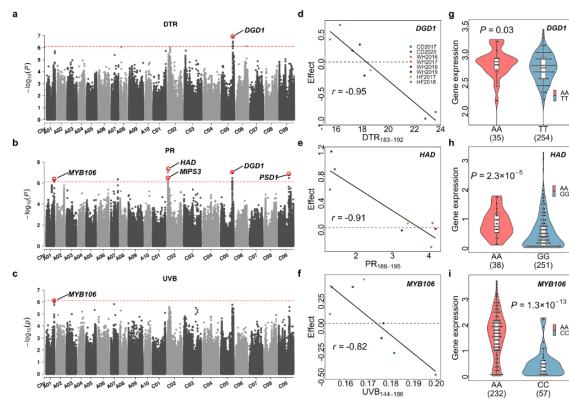


Fig. 5 Identification and characterization of genetic loci associated with phenotypic plasticity in seed oil content in *Brassica napus*. **a–c**, Manhattan plots showing the genomic regions associated with SOC phenotypic plasticity in response to the identified environmental index: DTR_{183–192} (**a**), PR_{166–195} (**b**) and UVB_{144–186} (**c**). Red dashed lines represent the genome-wide significance threshold. **d–f**, Genetic effect from *DGD1*, *HAD* or *MYB106* on variation for the indicated environmental index: DTR_{183–192} (**d**), PR_{166–195} (**e**) and UVB_{144–186} (**f**). **g–i**, Expression levels of the two alleles for the indicated gene in the *B. napus* diversity panel, as determined by abundances of transcripts. Significant differences ($p < 0.05$) were determined with a Wilcoxon test.

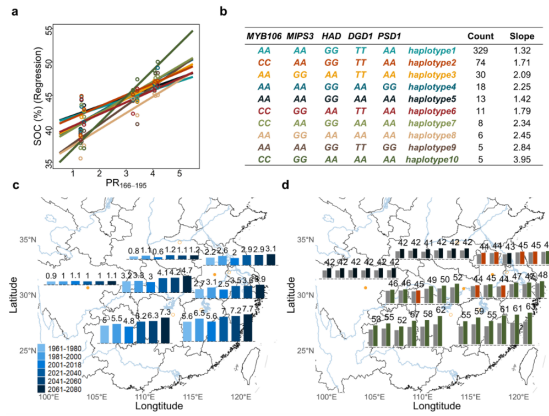


Fig. 6 Predicting optimal haplotypes across planting sites and time periods. a, Reaction norms of haplotypes showing SOC plasticity to the environmental index $PR_{166-195}$. **b,** List of 10 major haplotypes with their allele combinations at the five plasticity genes. **c,** Precipitation levels during the critical growth stage at seven planting sites from 1960 to 2080. **d,** Optimal haplotype with the highest SOC from 1960 to 2080, compared to the mean of all haplotypes (gray bar) at seven planting sites during different time periods.